Petroleum Science 18 (2021) 1127–1142

Contents lists available at ScienceDirect

Petroleum Science

journal homepage: www.keaipublishing.com/en/journals/petroleum-science

Original Paper

An improved data space inversion method to predict reservoir state fields via observed production data

Deng Liu [a, b], Xiang Rao [a, b, *], Hui Zhao [b, **], Yun-Feng Xu [b], Ru-Xiang Gong [c]

[a] Cooperative Innovation Center of Unconventional Oil and Gas (Ministry of Education & Hubei Province), Yangtze University, Wuhan, 434023, Hubei, PR China
[b] School of Petroleum Engineering, Yangtze University, Wuhan, 434023, Hubei, PR China
[c] CNOOC Oilfield Services Co., Ltd., Tianjin, 30000, PR China

ARTICLE INFO

Article history:
Received 9 November 2020
Accepted 5 March 2021
Available online 8 July 2021

Edited by: Yan-Hua Sun

Keywords:
Fossil fuels
Oil and gas reservoirs
Reservoir state fields
Production data
Data inversion method

ABSTRACT

A data-space inversion (DSI) method has been recently proposed and successfully applied to the history matching and production prediction of reservoirs. Based on Bayesian theory, DSI can directly and effectively obtain good posterior flow predictions without inversion of geological parameters of reservoir model.

This paper presents an improved DSI method to fast predict reservoir state fields (e.g. saturation and pressure profiles) via observed production data. Firstly, a large number of production curves and state data are generated by reservoir model simulation to expand the data space of original DSI. Then, efficient history matching only on the observed production data is carried out via the original DSI to obtain related parameters which reflects the weight of the real reservoir model relative to prior reservoir models. Finally, those parameters are used to predict the oil saturation and pressure profiles of the real reservoir model by combining large amounts of state data of prior reservoir models. Two examples including conventional heterogeneous and unconventional fractured reservoir are implemented to test the performances of predicting saturation and pressure profiles of this improved DSI method. Besides, this method is also tested in a real field and the obtained results show the high computational efficiency and high accuracy of the practical application of this method.

1. Introduction

Accurate estimation of state field of reservoir can help deploy the position of new drilling wells and production plans to improve reservoir development efficiency. In practice, accurate estimation obtained by engineers is depend on precise judgments of subsurface flow situation through a large amount of production and geological data. Rather, due to uncertainty of reservoir with high heterogeneity and flow complexity, it is usually a hard task to get available estimation in real time.

The history matching method based on a full-scale reservoir model can solve this problem (Evensen et al., 2007; Haugen et al., 2006; Li and Reynolds, 2011; Naevdal et al., 2002, 2003). As a model-driven method, the posterior model is obtained through adjusting the model parameters repeatedly to make its simulation results match the observation data (Brouwer et al., 2001). The corresponding state field can be calculated through simulator. However, history matching is a very hard and time-consuming work, which involves intensive use of computational resources with long-time repeated numerical simulation process. And the uncertainty of the reservoir model is hard to be quantified under limited collected data.

To reduce computational cost, the data-driven model is developed for quick production prediction to replace classical reservoir simulation (Araque-Martinez, 1993; Barros-Griffiths, 1998; Heffer et al., 1997; Jansen and Kelkar, 1997; Refunjol, 1996). The data-driven model does not require any prior knowledge of a detailed geological model but a large number of production data. The computational speed of the data-driven model is hundreds of times faster than

* Corresponding author. Cooperative Innovation Center of Unconventional Oil and Gas (Ministry of Education & Hubei Province), Yangtze University, Wuhan, 434023, Hubei, PR China.
** Corresponding author.
E-mail addresses: raoxiang0103@163.com (X. Rao), zhaohui@yangtzeu.edu.cn (H. Zhao).

https://doi.org/10.1016/j.petsci.2021.07.008

traditional numerical simulation. At present, the typical data-driven models such as the capacitance-resistance model (CRM) (Albertoni and Lake, 2003; Sayarpour et al., 2009; Tiab and Dinh, 2008; Yousef et al., 2005), inter-well numerical simulation model (INSIM) are applied successfully for two-phase (water/oil) flow simulation (Guo et al., 2018; Guo and Reynolds, 2019; Zhao et al., 2016, 2020). Nevertheless, most of data-driven models can only calculate pressure and saturation on well points and its connections.

As an alternative history matching method, the machine learning model can also generate reservoir prediction in a short time as long as we have enough training data (Rao et al., 2020b; Nguyen et al., 2011; Cao et al., 2015). Among the machine learning methods, the recurrent neural network (RNN) method is suitable for solving time series problems with regard to short-term prediction (Chaki et al., 2020). However, the construction of these models also relies on the information of the physical flow model. Recently, the long short-term memory (LSTM) method was applied to establish a model for predicting water saturation and pressure profiles (Zhang et al., 2019a). These machine-learning proxy models provide fast forecasts among input/output relations, but they require a large number of data to train the model, and the data preparation is very time-consuming sometimes.

Recently, a novel DSI method has been proposed and greatly improved the computational efficiency of history matching (Sun and Durlofsky, 2017; Sun et al., 2017). This method uses the production data of prior models to establish a proxy model with parameterization method. Different from machine learning model, this proxy model can measure the weight of the real model relative to each prior model. DSI only needs the prior model set which reflect the geological characteristics and its production performance data under simulation. Under the Bayesian framework, DSI can directly obtain the trustworthy production forecast by following the random maximum likelihood (RML) principle with no repeated numerical simulation process. Importantly, the posterior forecast can quantify uncertainty of reservoir system without constructing any posterior reservoir model.

Up to now, DSI method is mainly used to predict the production performance of reservoirs, and the related production optimization method has been formed (Jiang, 2018; Jiang et al., 2019). Nevertheless, due to the lack of the inversion of geological parameters (e.g., permeability profile, porosity profile and etc.), this method is extremely limited in the prediction of reservoir state fields (i.e., pressure profile, saturation profile and etc.). Additional, Sun and Durlofsky (2019) used the DSI method to predict carbon dioxide plume location given the pressure and saturation data at observation wells. Application of DSI with optimal monitoring wells is shown to consistently reduce the posterior variance of average CO_2 saturation in the top layer, and provide detailed CO_2 saturation fields in reasonable correspondence with the true saturation field. However, DSI have not been applied for predicting real-time oil saturation and pressure field of a real reservoir.

This paper introduces an improved DSI method to quickly predict reservoir state fields by using prior geological model simulation results and the observed production data. Compared with the original DSI method, the reservoir state data is added into the data space as extra data variables. The posterior state prediction is extrapolated from the proxy model, but the part of reservoir state field in data space does not participate in history matching. In this paper, we improve the optimization algorithm and use SPSA algorithm to avoid overfitting problem. Two numerical examples including conventional and unconventional reservoir models are carried out to valid the good performances and generality of this method. Moreover, the improved DSI method is also used for a real field case and the obtained posterior forecasts shows the practicability of this method.

2. Methodology

Compared with the original DSI (Sun and Durlofsky, 2017), the improved DSI puts the state data of reservoir as additional data variables into data space. Only the observed production data are used for history matching and we can use the conditional proxy model to extrapolate the posterior state field. Therefore, the history matching process is basically consistent with DSI.

2.1. The data-space formulation

Based on random sampling, N_r prior reservoir models with geological characteristics are generated. Let $\boldsymbol{m}\in R^{N_m\times 1}$ represents the geological parameters of one of those prior reservoir models. We designate $\boldsymbol{d}_{state}\in R^{N_{state}\times 1}$ to represent the state data of one reservoir model which contains N_{state}-dimensional column of the form

$$\boldsymbol{d}_{state}=\left[\boldsymbol{d}_{state,1}^{T},\ \boldsymbol{d}_{state,2}^{T},\ \ldots,\ \boldsymbol{d}_{state,N_k}^{T},\ \ldots,\ \boldsymbol{d}_{state,N_h}^{T},\ \ldots,\ \boldsymbol{d}_{state,N_t}^{T}\right]^{T} \tag{1}$$

where the subscript k is the kth control time step, $\boldsymbol{d}_{state,N_k}^{T}$ is the vector of the state data at time step k, N_h represents the number of time steps in the history matching period, N_t is the total number of time steps including history matching and forecast period, $N_{state}=2{*}N_m{*}N_t$. We also designate $\boldsymbol{d}\in R^{N_d\times 1}$ to represent the production data which are the other data variables in the data space, which contains oil production rate, bottom hole pressure, etc.

$$\boldsymbol{d}=\left[\boldsymbol{d}_1^{T},\ \boldsymbol{d}_2^{T},\ \ldots,\ \boldsymbol{d}_{N_k}^{T},\ \ldots,\ \boldsymbol{d}_{N_h}^{T},\ \ldots,\boldsymbol{d}_{N_t}^{T}\right]^{T}=\left[\boldsymbol{d}_{hm}^{T},\ \boldsymbol{d}_{p}^{T}\right]^{T} \tag{2}$$

where $\boldsymbol{d}_{hm}\in R^{N_{hm}\times 1}$ is the production data in history matching period and $\boldsymbol{d}_p\in R^{N_p\times 1}$ is the production data in forecast period, $N_{hm}+N_P=N_d$. Assuming that there are n production indicators, then $N_d=n{*}N_t$. The $\boldsymbol{d}_{state}$ and $\boldsymbol{d}$ of each prior model can be calculated numerically via

$$(\boldsymbol{d}_{state},\ \boldsymbol{d})_i=g(\boldsymbol{m}_i),\quad i=1,\ 2,\ \ldots,\ N_r \tag{3}$$

where $g(\cdot)$ is the numerical simulator. In the original DSI (Sun and Durlofsky, 2017), the data space only contains production data. For the improved DSI method, its goal is to predict production performances and state fields at the same time. Therefore, state variables are added into the data space, that is

$$\left(\boldsymbol{d}_{full}\right)_i=(\boldsymbol{d}_{state},\ \boldsymbol{d})_i, i=1,\ 2,\ \ldots,\ N_r \tag{4}$$

where $\boldsymbol{d}_{full}\in R^{N_f\times 1}$ represents the data space which includes the data variables in history matching and prediction period, $N_f=N_d+N_{state}$. In practice, the observed production data is known, but the state fields of subface cannot be measured. Therefore, we take only the observed production data to be history matching and generate the trained proxy model. The state fields are then calculated rapidly by the trained proxy model. Thus, the history matching process in this paper is similar to that in the original DSI method. The next section briefly introduces the history matching process of the improved DSI.

2.2. Inversion procedure

Let $\boldsymbol{d}_{obs}\in R^{N_{hm}\times 1}$ denote the vector of the observed production data and $\boldsymbol{d}_{obs}$ is equal to $\boldsymbol{d}_{hm}$, the relationship between $\boldsymbol{d}_{full}$ and $\boldsymbol{d}_{obs}$

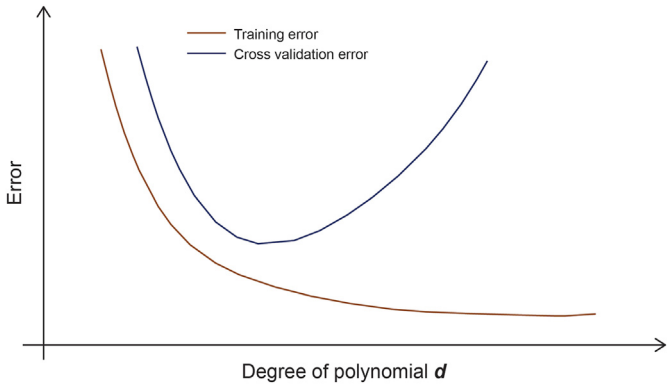

Fig. 1. Overfitting phenomenon in the process of training for the machine learning model.

can be represented as

$$\boldsymbol{d}_{\text{obs}} = \boldsymbol{H}\boldsymbol{d}_{\text{full}} + \varepsilon \tag{5}$$

where $\varepsilon \in R^{N_{\text{hm}} \times 1}$ is the vector of measurement errors of the observed data, which is assumed to be Gaussian random variables with mean 0 and covariance matrix $\boldsymbol{C}_{\text{D}}$, $\boldsymbol{C}_{\text{D}} \in R^{N_{\text{hm}} \times N_{\text{hm}}}$. Besides, $\boldsymbol{H} \in R^{N_{\text{hm}} \times N_{\text{f}}}$ is applied to extract the historical production data from $\boldsymbol{d}_{\text{full}}$. Similar to $\boldsymbol{H}$ matrix, we also define $\boldsymbol{E} \in R^{N_{\text{d}} \times N_{\text{f}}}$ to extract the total production data from $\boldsymbol{d}_{\text{full}}$, it can be expressed as

$$\boldsymbol{d} = \boldsymbol{E}\boldsymbol{d}_{\text{full}} \tag{6}$$

Therefore, under Bayesian framework, it is straightforward to determine the likelihood of $\boldsymbol{d}$, that is

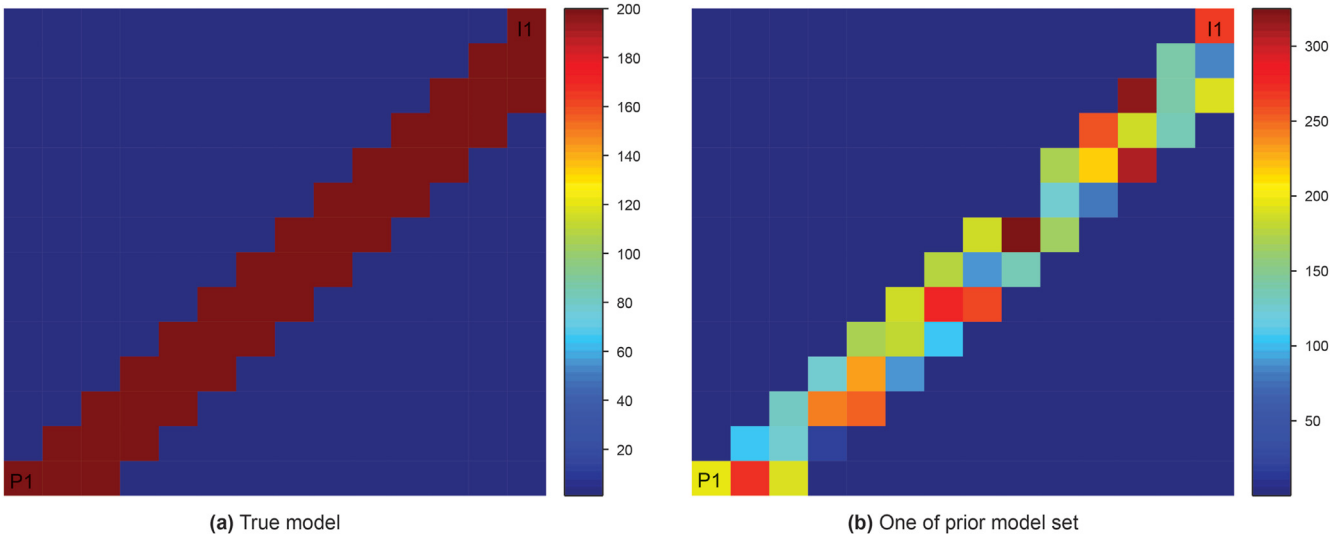

(a) True model **(b)** One of prior model set

Fig. 2. Permeability field (Permeability, mD).

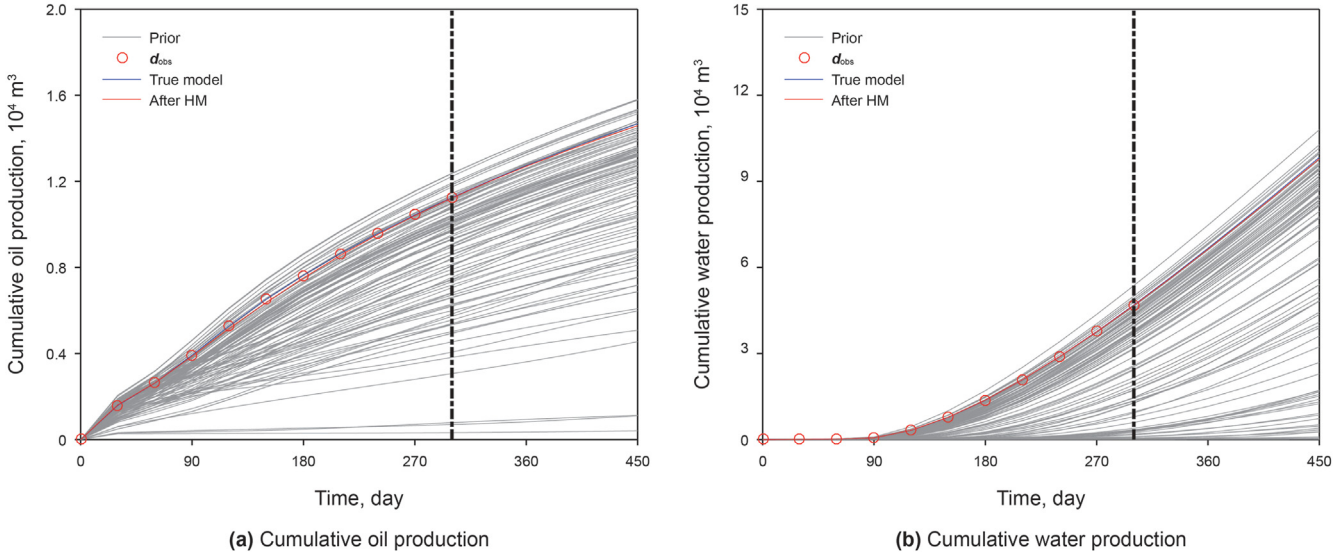

(a) Cumulative oil production **(b)** Cumulative water production

Fig. 3. Comparisons of production data before and after history matching.

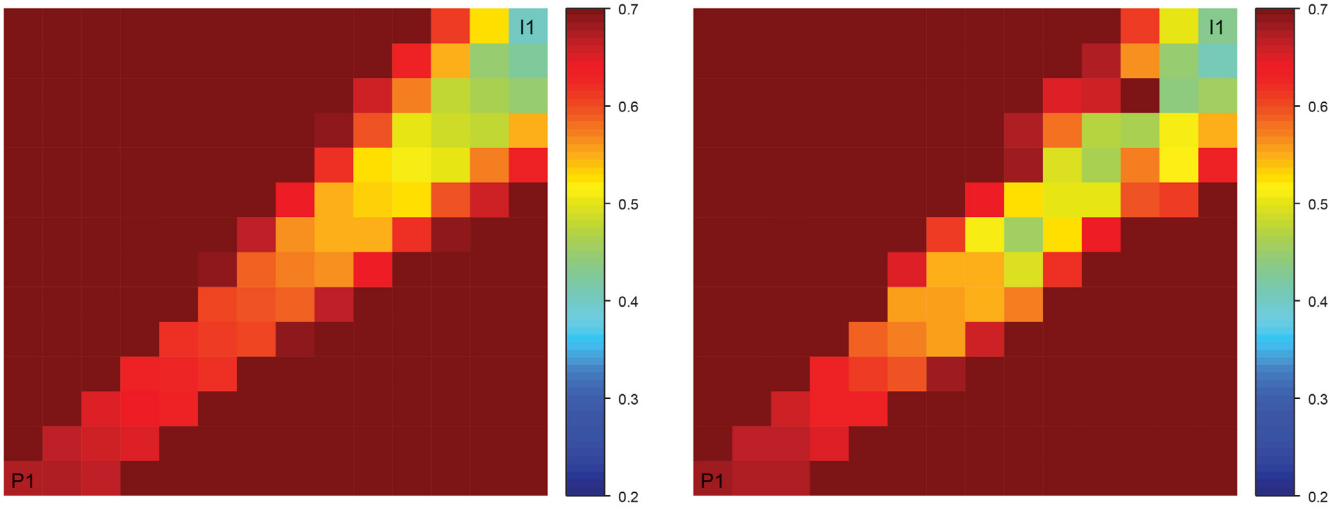

(a) 150th day

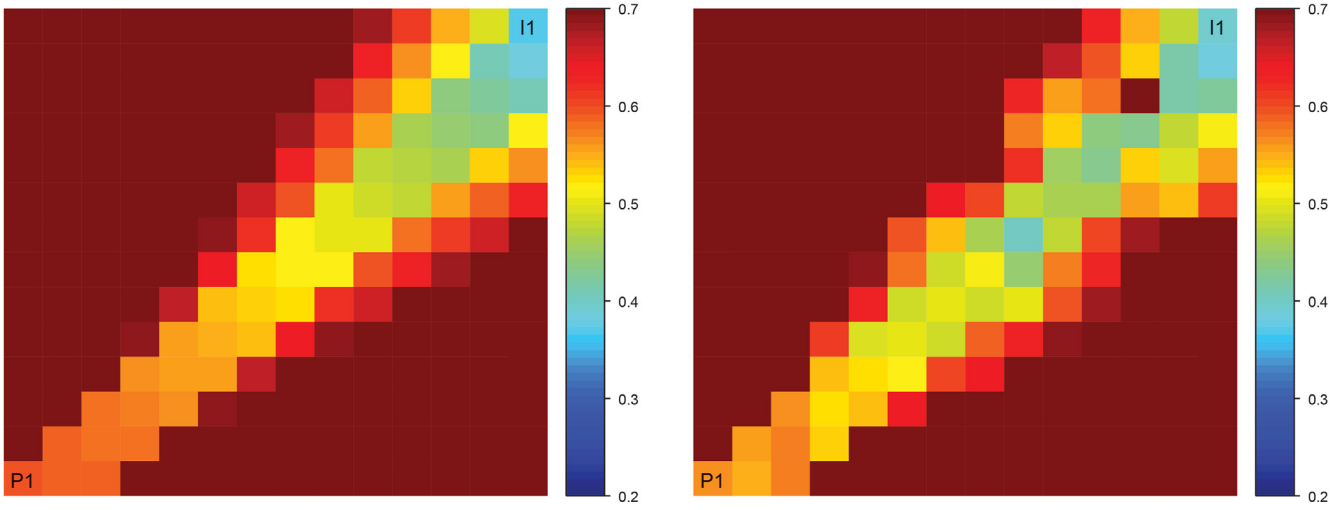

(b) 300th day

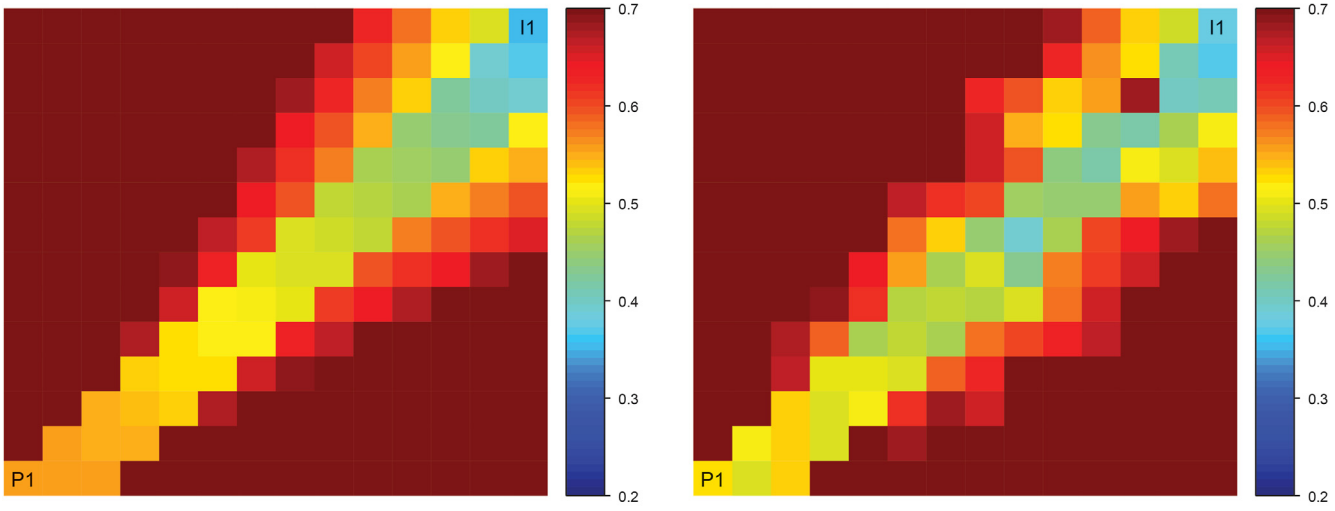

(c) 450th day

Fig. 4. Comparisons of the oil saturation profiles at different time in the case of water flooding reservoir.

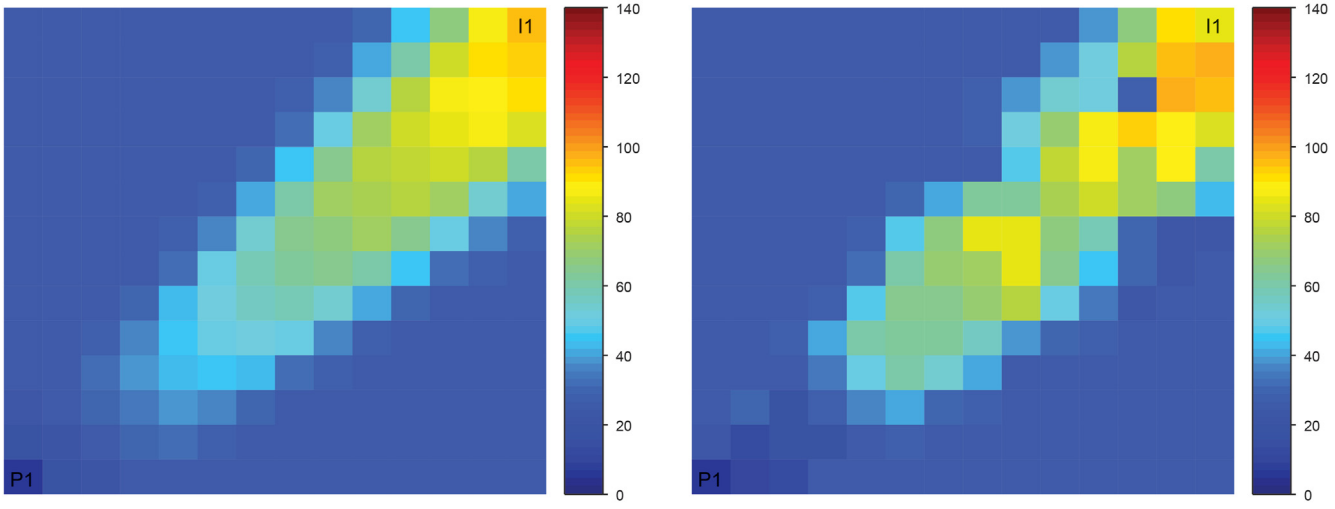

(a) 150th day

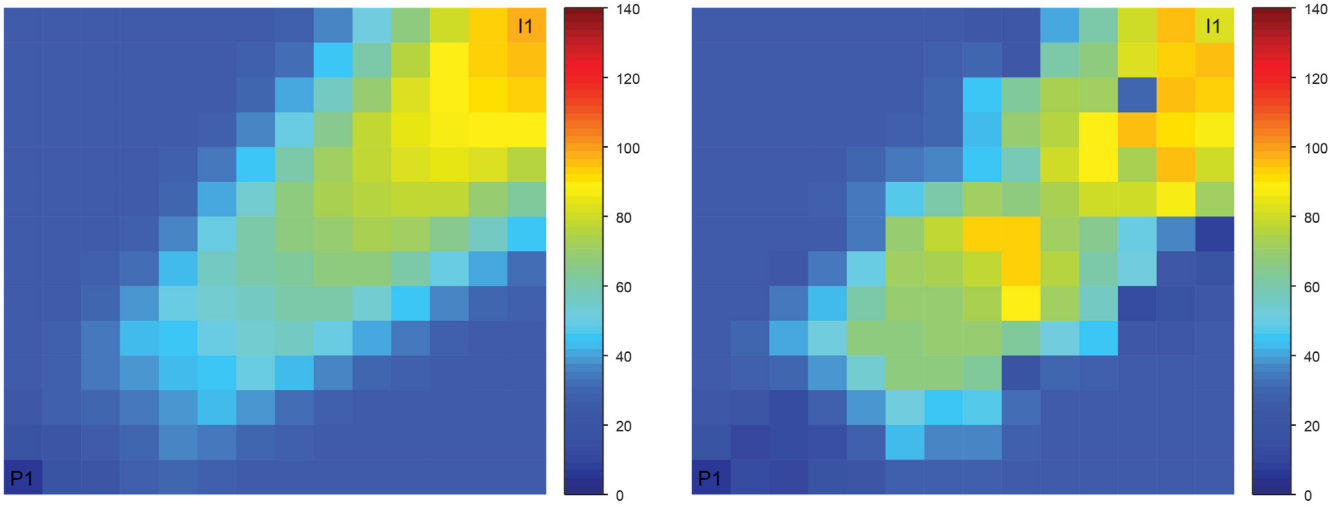

(b) 300th day

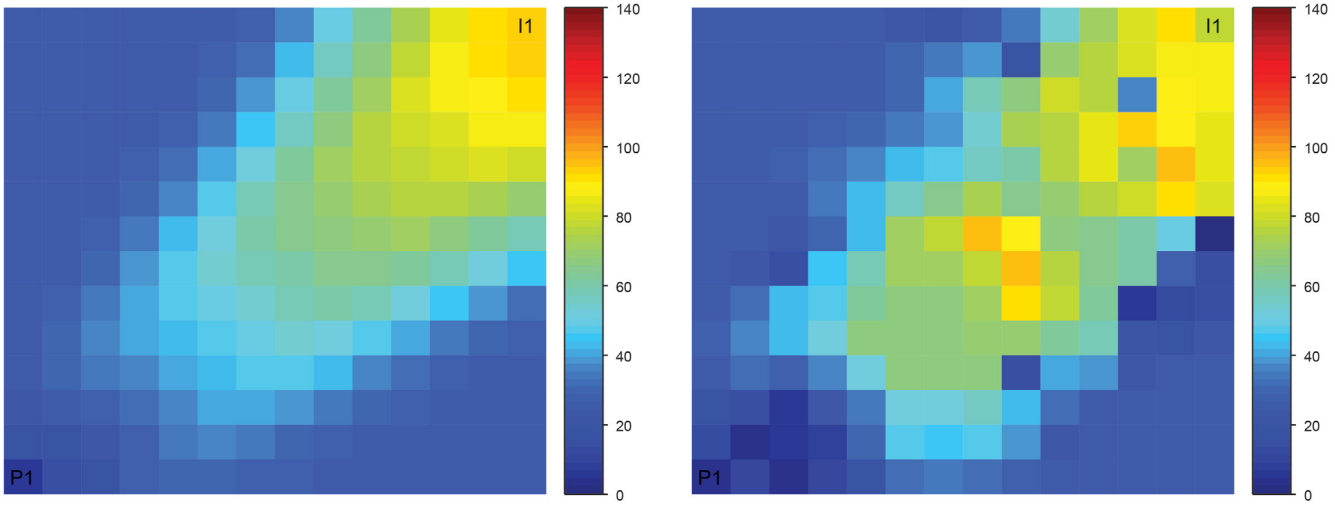

(c) 450th day

Fig. 5. Comparisons of the pressure profiles at different time in the case of water flooding reservoir (Pressure, MPa).

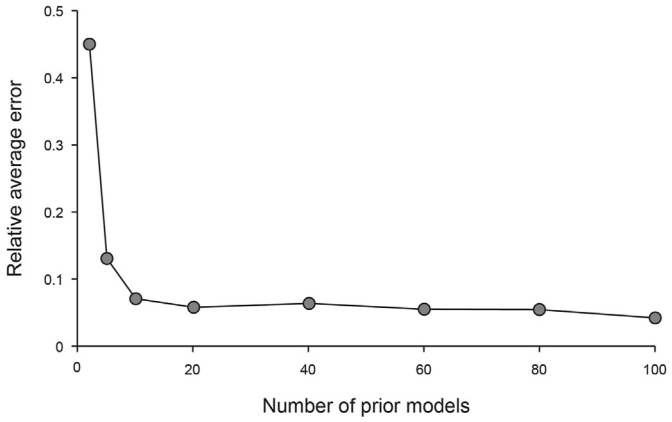

Fig. 6. The relationship between the number of prior models and the relative error.

$$O(\boldsymbol{d}) = \left(\boldsymbol{E}\boldsymbol{d}_{\text{full}} - \boldsymbol{d}_{\text{prior}}\right)^{\text{T}} \boldsymbol{C}_{\text{d}}^{-1} \left(\boldsymbol{E}\boldsymbol{d}_{\text{full}} - \boldsymbol{d}_{\text{prior}}\right) + \left(\boldsymbol{H}\boldsymbol{d}_{\text{full}} - \boldsymbol{d}_{\text{obs}}\right)^{\text{T}} \boldsymbol{C}_{\text{D}}^{-1} \left(\boldsymbol{H}\boldsymbol{d}_{\text{full}} - \boldsymbol{d}_{\text{obs}}\right) \tag{7}$$

where $\boldsymbol{d}_{\text{prior}} \in R^{N_{\text{d}} \times 1}$ and $\boldsymbol{C}_{\text{d}} \in R^{N_{\text{d}} \times N_{\text{d}}}$ represent the mean of and covariance of $\boldsymbol{d}$, respectively, that are,

$$\boldsymbol{d}_{\text{prior}} = \frac{1}{N_{\text{r}}} \sum_{i=1}^{N_{\text{r}}} \boldsymbol{d}_i \tag{8}$$

and

$$\boldsymbol{C}_{\text{d}} = \frac{1}{N_{\text{r}} - 1} \sum_{i=1}^{N_{\text{r}}} \left[\boldsymbol{d}_i - \boldsymbol{d}_{\text{prior}}\right] \left[\boldsymbol{d}_i - \boldsymbol{d}_{\text{prior}}\right]^{\text{T}} \tag{9}$$

Posterior production predictions can be obtained through the minimization of Eq. (7). However, due to long production history for a real field, it is still difficult to solve the covariance matrix $\boldsymbol{C}_{\text{d}}^{-1}$ with high dimensions of $\boldsymbol{d}$. Sun and Durlofsky (2017) introduced the parameterization method of $\boldsymbol{d}$ to construct a proxy model and avoid the calculation of $\boldsymbol{C}_{\text{d}}^{-1}$. The conditional proxy model can calculate posterior production predictions after history matching. The parameters in the conditional proxy model basically reflect the weight of the real model relative to the prior models.

2.3. Reparameterization methods

In the original DSI, Sun and Durlofsky (2017) applied PCA method to parameterize the data space for avoiding the calculation of $\boldsymbol{C}_{\text{d}}^{-1}$. Singular value decomposition is carried out for $\boldsymbol{X} = \left[\boldsymbol{d}_1 - \boldsymbol{d}_{\text{prior}},\ \boldsymbol{d}_2 - \boldsymbol{d}_{\text{prior}},\ \ldots,\ \boldsymbol{d}_{N_{\text{r}}} - \boldsymbol{d}_{\text{prior}}\right]$, which denotes

$$\boldsymbol{X} \Big/ \sqrt{N_{\text{r}} - 1} = \boldsymbol{U}\boldsymbol{\Sigma}\boldsymbol{V}^{\text{T}} = \boldsymbol{\Phi}\boldsymbol{V}^{\text{T}} \tag{10}$$

where $\boldsymbol{U} \in R^{N_{\text{d}} \times N_{\text{d}}}$ is the unitary matrix containing the left singular value of $\boldsymbol{X}/\sqrt{N_{\text{r}} - 1}$, $\boldsymbol{\Sigma} \in R^{N_{\text{d}} \times N_{\text{r}}}$ is the diagonal matrix containing non-zero singular values of $\boldsymbol{X}/\sqrt{N_{\text{r}} - 1}$, $\boldsymbol{V} \in R^{N_{\text{r}} \times N_{\text{r}}}$ is the unitary matrix containing the right singular value of $\boldsymbol{X}/\sqrt{N_{\text{r}} - 1}$, $\boldsymbol{\Phi} \in R^{N_{\text{d}} \times N_{\text{r}}}$ is the basis matrix, $\boldsymbol{\Phi} = \boldsymbol{U}\boldsymbol{\Sigma}$. Then, an 'energy' criterion method was applied to remain the largest N_{s} number of singular values in $\boldsymbol{\Sigma}$ to preserve data characteristics. In this case, let $\boldsymbol{\Phi}_{\text{PCA}} \in R^{N_{\text{d}} \times N_{\text{s}}}$ denote the transformed basis matrix, and for any production data $\boldsymbol{d}$, it can be expressed as

$$\boldsymbol{d} \approx \boldsymbol{\Phi}_{\text{PCA}} \xi + \boldsymbol{d}_{\text{prior}} \tag{11}$$

where $\xi \in R^{N_{\text{s}} \times 1}$ can be regarded as the proxy of the production data, whose order is much lower than that of geological parameters. Through the parameterization method, DSI can avoid the calculation of $\boldsymbol{C}_{\text{d}}^{-1}$ and solve the optimization problem in N_{s}-dimensional. The target function can be expressed as

$$O(\xi) = \left(\boldsymbol{\Phi}_{\text{PCA}}^{\text{H}} \xi + \boldsymbol{d}_{\text{prior}}^{\text{H}} - \boldsymbol{d}_{\text{obs}}\right)^{\text{T}} \boldsymbol{C}_{\text{D}}^{-1} \left(\boldsymbol{\Phi}_{\text{PCA}}^{\text{H}} \xi + \mathbf{d}_{\text{prior}}^{\text{H}} - \boldsymbol{d}_{\text{obs}}\right) + \xi^{\text{T}} \xi \tag{12}$$

where $\boldsymbol{\Phi}_{\text{PCA}}^{\text{H}} \in R^{N_{\text{hm}} \times N_{\text{s}}}$ and $\boldsymbol{d}_{\text{prior}}^{\text{H}} \in R^{N_{\text{hm}} \times 1}$ represent the historical portion of $\boldsymbol{\Phi}_{\text{PCA}}$ and $\boldsymbol{d}_{\text{prior}}$. The optimization problem is transformed into that to find a best posterior estimation of ξ to minimize the target function. Served as a proxy model, the elements of the conditional ξ can be regarded as the optimal weight coefficient of production data, which relates prior model to true model.

Sun and Durlofsky (2017) indicated that the application of PCA method may lead to unphysical values for production predictions. In practice, it usually occurs in the period before water breakthrough. For this reason, some mapping operations based on shifting and stretching the time series were adopted to transform the prior production data into approximate Gaussian field. But it became more complex for the implementation of DSI when well controls change frequently. Histogram transformation was implemented on PCA data and got good result (Sun et al., 2017). In this paper, to simplify the calculation process, we directly parameterize production data in the section of the data space to avoid computing $\boldsymbol{C}_{\text{d}}^{-1}$. We redefine the basis matrix of $\boldsymbol{d}$,$\boldsymbol{\Phi} = \boldsymbol{X}/\sqrt{N_{\text{r}} - 1}$,$\boldsymbol{\Phi} \in R^{N_{\text{d}} \times N_{\text{r}}}$, therefore,

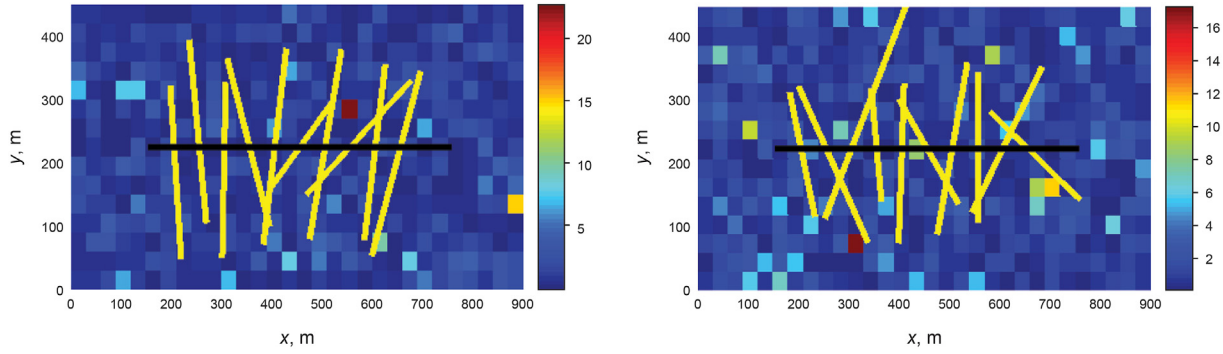

Fig. 7. Sketch of fracture geometry and matrix permeability (Permeability, mD).

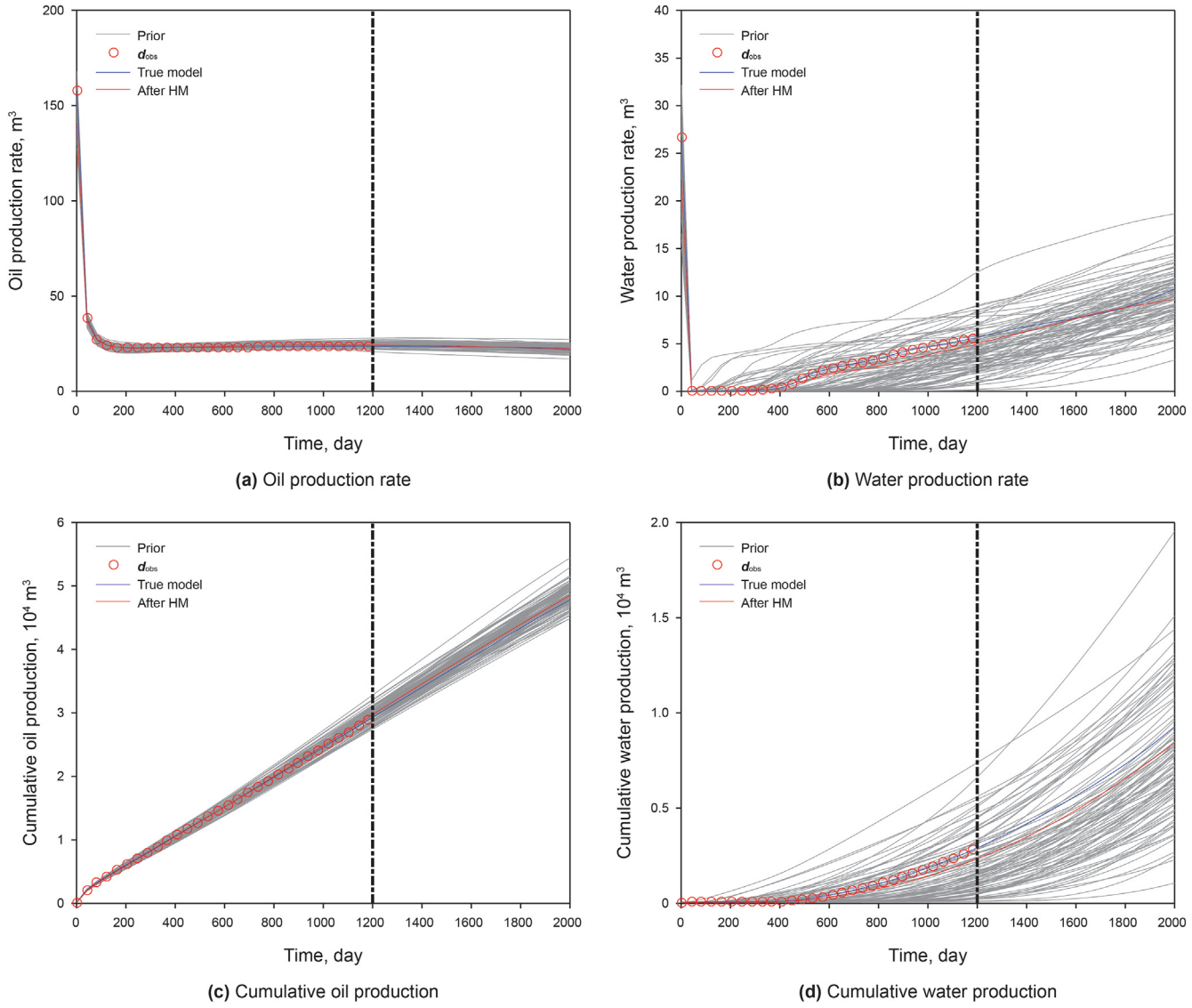

Fig. 8. The comparisons of production data before and after history matching.

$$\boldsymbol{d} = \boldsymbol{\Phi}\boldsymbol{\xi} + \boldsymbol{d}_{\text{prior}} \tag{13}$$

where $\xi \in R^{N_r \times 1}$, if for $\boldsymbol{d}_i$, the ith component of the corresponding ξ_i is equal to $\sqrt{N_r - 1}$, and other components are zero. Besides, $\boldsymbol{C}_d$ can be expressed as

$$\boldsymbol{C}_d = \boldsymbol{\Phi}\boldsymbol{\Phi}^T \tag{14}$$

thus

$$(\boldsymbol{d} - \boldsymbol{d}_{\text{prior}})^T \boldsymbol{C}_d^{-1} (\boldsymbol{d} - \boldsymbol{d}_{\text{prior}}) = (\boldsymbol{\Phi}\boldsymbol{\xi})^T \cdot \left(\boldsymbol{\Phi}\boldsymbol{\Phi}^T\right)^{-1} \cdot (\boldsymbol{\Phi}\boldsymbol{\xi}) = \xi^T \xi \tag{15}$$

In this way, the calculation of the covariance matrix $\boldsymbol{C}_d^{-1}$ is avoided. Besides, the first-order image gradient of the objective function can be obtained. In history matching process, the elements of the conditional ξ is the optimal weight coefficient of production data, which relate prior model to true model. The weight coefficient reflects the uncertainty of reservoir, including the uncertainty of reservoir model state field. Therefore, posterior state fields can be predicted by

$$\boldsymbol{d}_{\text{state}} = \boldsymbol{\Phi}_{\text{state}}\boldsymbol{\xi} + \boldsymbol{d}_{\text{state,prior}} \tag{16}$$

where $\boldsymbol{d}_{\text{state,prior}} \in R^{N_{\text{state}} \times 1}$ and $\boldsymbol{\Phi}_{\text{state}} \in R^{N_{\text{state}} \times N_r}$ represent the mean and the basis matrix of $\mathbf{d}_{\text{state}}$, respectively, that are

$$\boldsymbol{d}_{\text{state,prior}} = \frac{1}{N_r} \sum_{i=1}^{N_r} d_{\text{state},i} \tag{17}$$

and

$$\boldsymbol{\Phi}_{\text{state}} = \boldsymbol{X}_{\text{state}} \Big/ \sqrt{N_r - 1} \tag{18}$$

$$\boldsymbol{X}_{\text{state}} = \left[\boldsymbol{d}_{\text{state},1} - \boldsymbol{d}_{\text{state,prior}}, \boldsymbol{d}_{\text{state},2} - \boldsymbol{d}_{\text{state,prior}}, \ldots, \boldsymbol{d}_{\text{state},N_r} - \boldsymbol{d}_{\text{state,prior}}\right]$$

The objective function can be expressed as

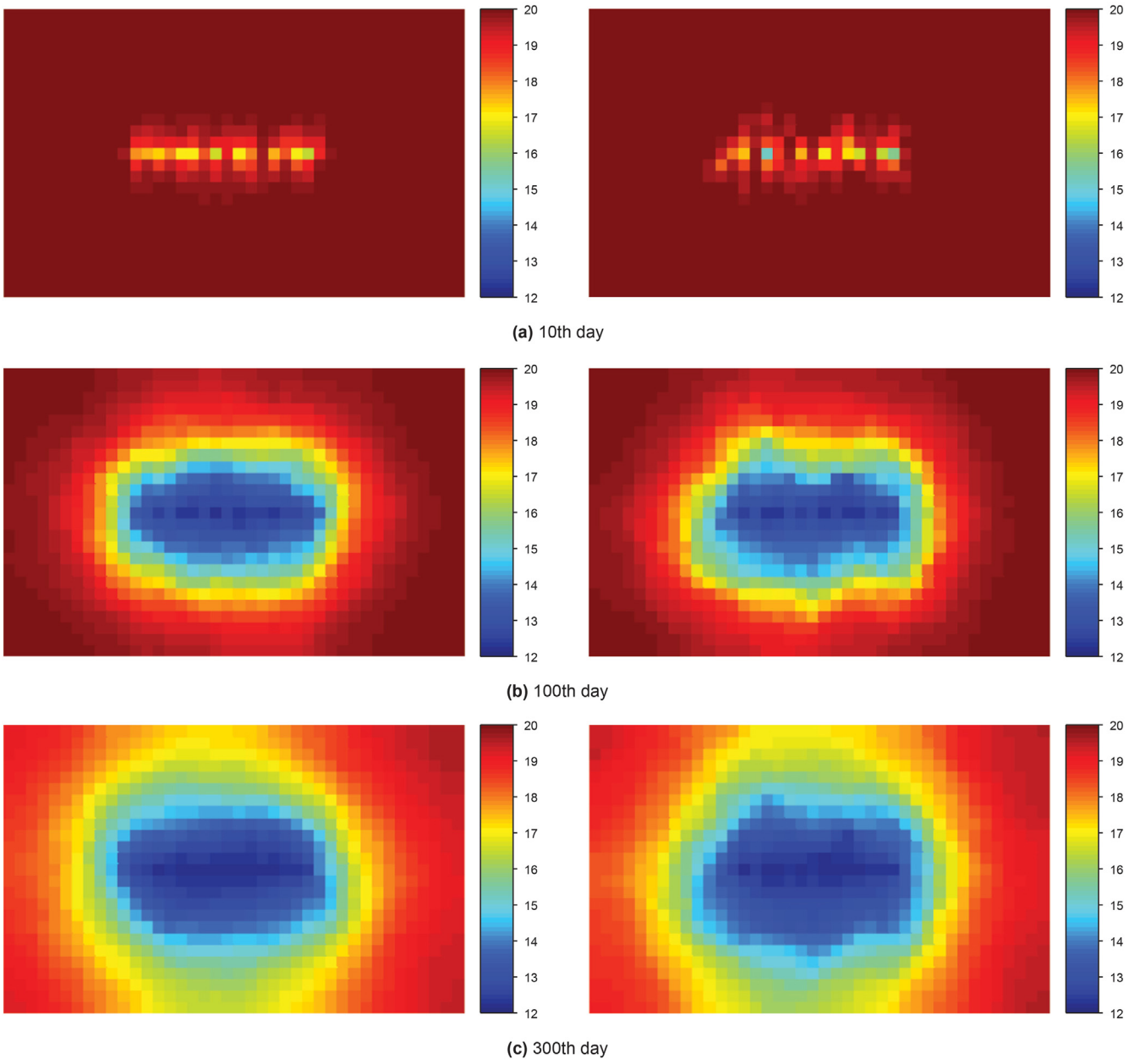

Fig. 9. The comparisons of the pressure profiles at different time in the case of depletion development (Pressure, MPa).

$$O(\xi) = \left(\boldsymbol{\Phi}^{\mathrm{H}}\xi + \boldsymbol{d}^{\mathrm{H}}_{\mathrm{prior}} - \boldsymbol{d}_{\mathrm{obs}}\right)^{\mathrm{T}} \boldsymbol{C}_{\mathrm{D}}^{-1}\left(\boldsymbol{\Phi}^{\mathrm{H}}\xi + \boldsymbol{d}^{\mathrm{H}}_{\mathrm{prior}} - \boldsymbol{d}_{\mathrm{obs}}\right) + \xi^{\mathrm{T}}\xi \tag{19}$$

where $\boldsymbol{\Phi}^{\mathrm{H}} \in R^{N_{\mathrm{hm}} \times N_{\mathrm{r}}}$ and $\boldsymbol{d}^{\mathrm{H}}_{\mathrm{prior}} \in R^{N_{\mathrm{hm}} \times 1}$ represent the historical portion of $\boldsymbol{\Phi}$ and $\boldsymbol{d}_{\mathrm{prior}}$, respectively. Random maximum likelihood method (RML) is introduced to sample the posterior forecast with gradient algorithm (Sun and Durlofsky, 2017). Each RML sample is generated by minimizing Eq. (20) given by

$$O(\xi) = \left(\boldsymbol{\Phi}^{\mathrm{H}}\xi + \boldsymbol{d}^{\mathrm{H}}_{\mathrm{prior}} - \boldsymbol{d}^{*}_{\mathrm{obs}}\right)^{\mathrm{T}} \boldsymbol{C}_{\mathrm{D}}^{-1}\left(\boldsymbol{\Phi}^{\mathrm{H}}\xi + \boldsymbol{d}^{\mathrm{H}}_{\mathrm{prior}} - \boldsymbol{d}^{*}_{\mathrm{obs}}\right) + (\xi - \xi^{*})^{\mathrm{T}}(\xi - \xi^{*}) \tag{20}$$

where $\xi^{*} \in R^{N_{\mathrm{r}} \times 1}$ is sampled from the standard normal field $N[0, \boldsymbol{I}]$, $\boldsymbol{d}^{*}_{\mathrm{obs}} \in R^{N_{\mathrm{hm}} \times 1}$ is the perturbed observation sampled from the Gaussian distribution $N[\boldsymbol{d}_{\mathrm{obs}}, \boldsymbol{C}_{\mathrm{D}}]$. In this paper, simultaneous perturbation stochastic approximation (SPSA) algorithm is adopted for solving this problem. Because the gradient of SPSA deviates slightly from the real gradient, the posterior forecast derived by SPSA can also approximately quantify uncertainty. In addition, the application of SPSA can avoid over fitting phenomenon. We will introduce the reason about algorithm selection in the next section.

2.4. Algorithm selection

The gradient algorithm is used to solve the above optimization problem (Sun and and Durlofsky, 2017), but the application of the gradient algorithm often leads to overfitting phenomenon in the history matching procedure. This phenomenon is similar to the overtraining result of machine learning model. Fig. 1 demonstrates the correlation between the training and cross validation error in training process. The training error of the model on the training data

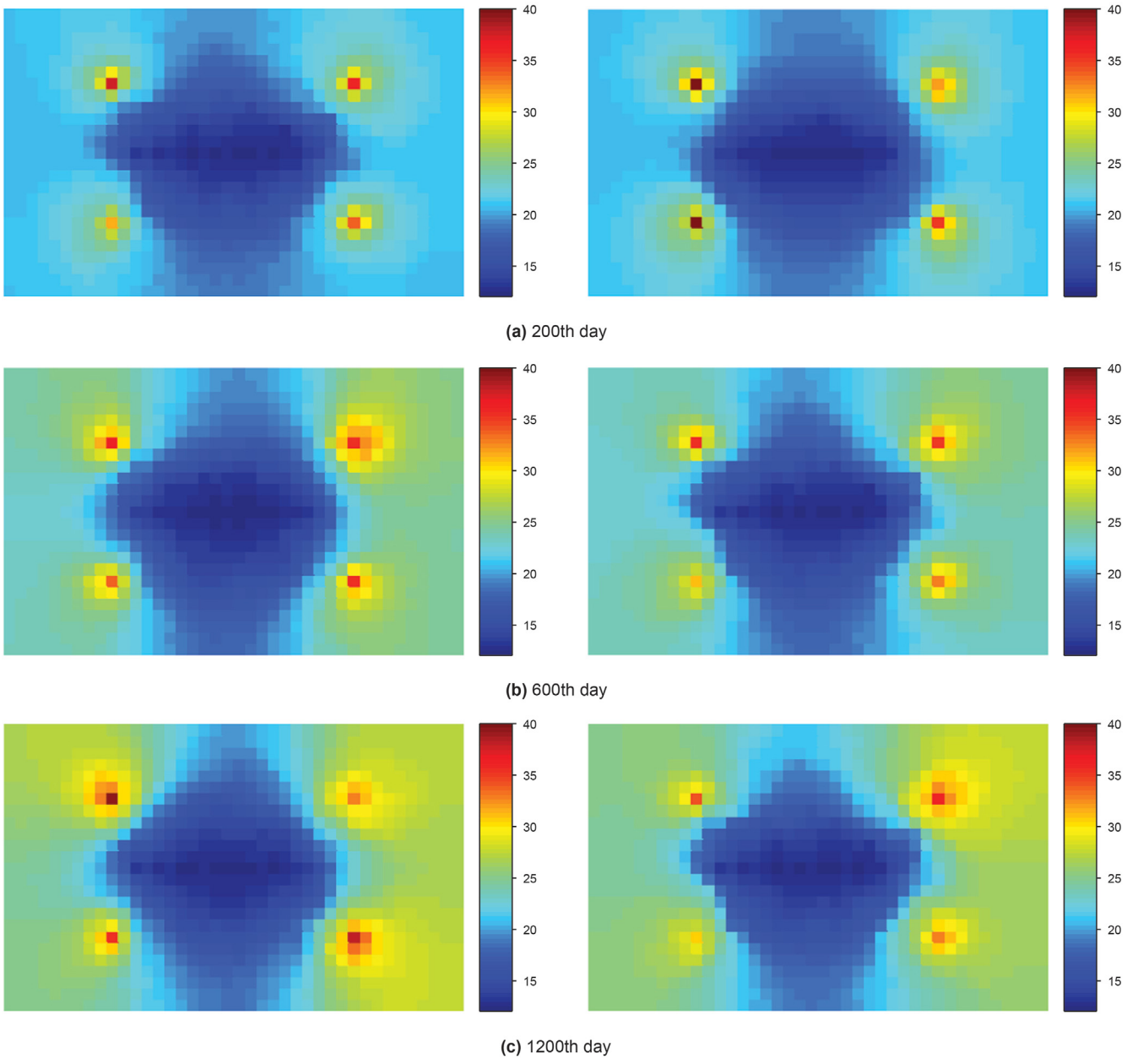

Fig. 10. The comparisons of the pressure profiles at different time in the case of water flooding reservoir (Pressure, MPa).

set will gradually decrease during the training period. However, as the complexity of the model increases, the error of the training model on the verification set will go up at the same time. When the gradient algorithm is applied, it achieves great results in history matching period. In contrast, the deviation from the true data in the forecast period is large and often leads to unpractical data.

Recently, Lima et al. (2020) used the DSI-ESMDA method to assimilate the observed data and the posterior forecast is more robust than the original DSI. Importantly, the localization method is adopted to revise the gradient to approximate the real gradient in model updating process, which significantly improve the quality of forecast results.

In this paper, we apply the SPSA algorithm (Spall 1992, 2000, 2000; Wang et al., 2009) to solve the optimization problem and improve the generalization ability of the proxy model. The gradient of SPSA is obtained by synchronous disturbance for all the control variables and the calculation of the objective function value. Although the disturbance gradient is random, its expected value is the real gradient. For the SPSA algorithm used in this paper, the early stopping method in the machine learning procedure is also adopted. In this method, the number of iterations is truncated to prevent overfitting before the convergence of value of target function. More details and parameter settings about SPSA algorithm are given in Appendix.

2.5. Selection of the prior models

Good training data can improve the generalization ability of the model and help to predict the dynamic state field of reservoir. Sun and Durlofsky (2017) used rejection sampling to screen data curves of prior reservoir realizations which are quite deviated from the observed data. In this paper, we adopt a similar method, the process is given as follows:

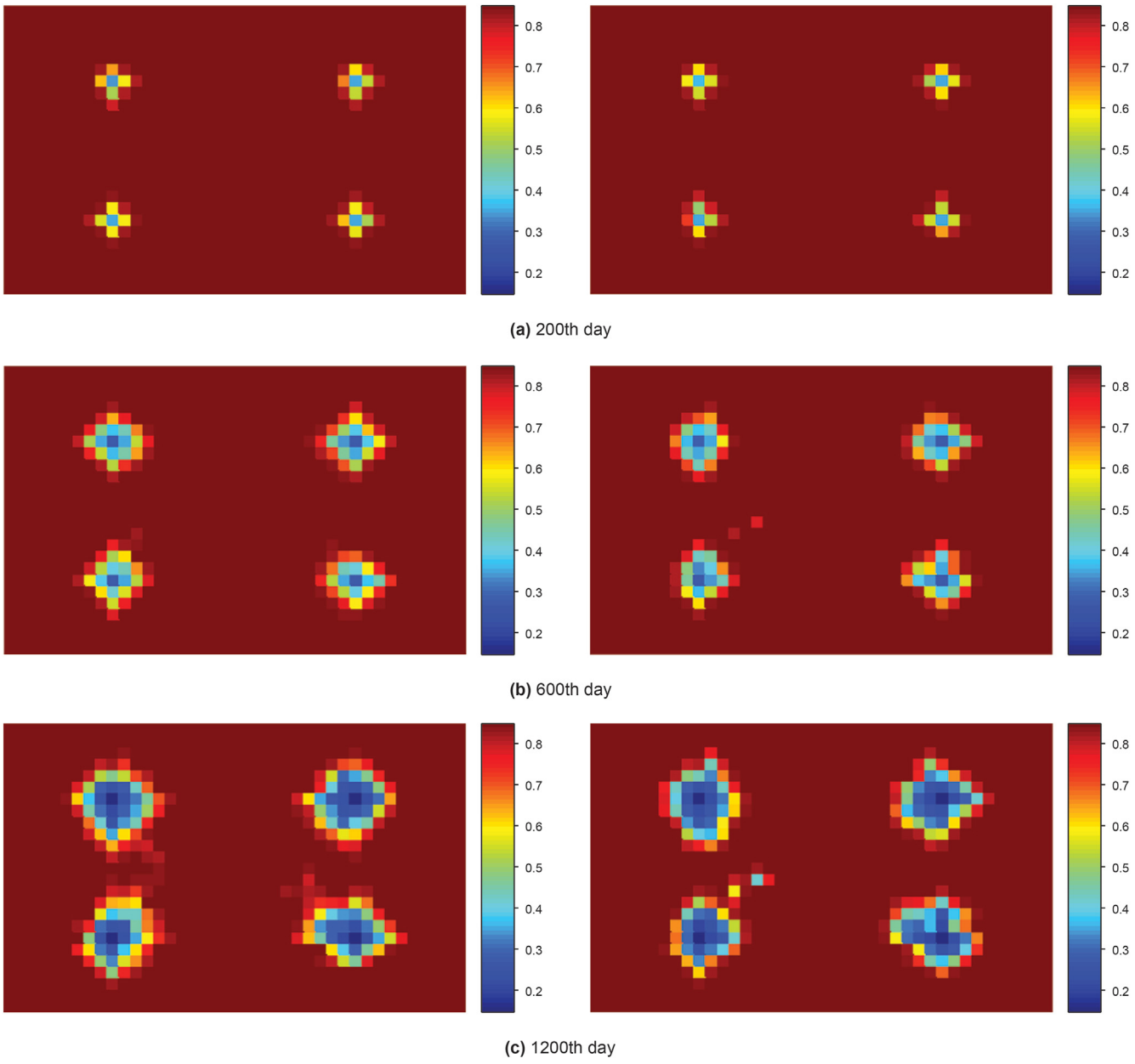

Fig. 11. The comparisons of the oil saturation profiles at different time in the case of water flooding reservoir.

(1) Generate an ensemble of prior reservoir realizations based on geological information.
(2) Randomly sampling p from the standard normal distribution $N(0,\ 1)$.
(3) Accept reservoir realizations if $p \leq L(\boldsymbol{m})$. The likelihood function is defined as

$$L(\boldsymbol{m}) = \sqrt{2\pi}\cdot\frac{\|g(\boldsymbol{m}) - \boldsymbol{d}_{\text{obs}}\|^2}{\|\boldsymbol{d}_{\text{obs}}\|^2} \tag{21}$$

2.6. Summary of the improved DSI method

This section summarizes the specific steps of the improved DSI method as follows:

Step 1. Generate some prior models by randomly sampling on geological parameters.

Step 2. Perform simulation on prior models and obtain production and state data in the lifetime of reservoir.

Step 3. Select the production and state data to form $\boldsymbol{d}_{\text{full}}$ (shown in Eq. (4)) and apply parameterization method to construct the proxy model through $\boldsymbol{d}_{\text{full}}$ in Eq. (13).

Step 4. Perform history matching and apply SPSA algorithm to solve the optimization problem in Eq. (19), then obtain the posterior parameter ξ.

Step 5. By Eq. (16), using ξ and $\boldsymbol{d}_{\text{state}}$ formed from state fields data to predict the pressure or saturation profiles of the real reservoir model.

The whole history matching process of DSI is efficient because the dimension of variables is low and repeated numerical

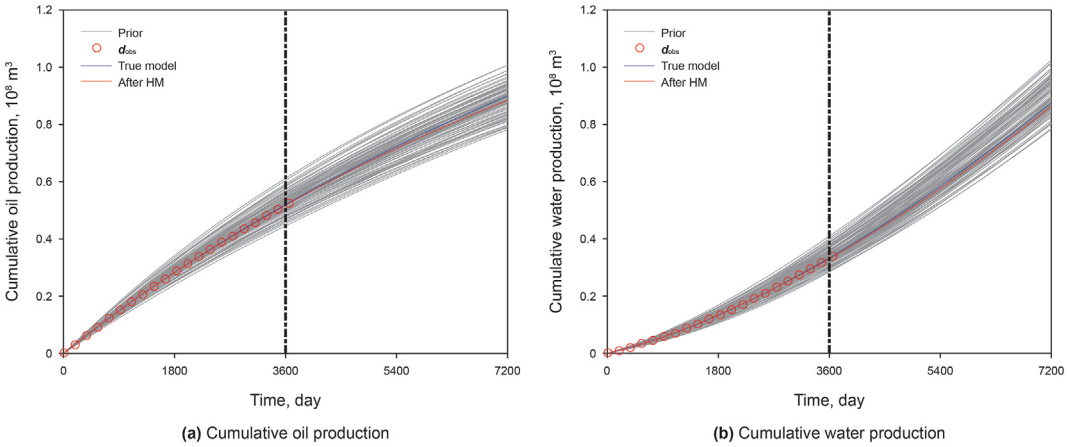

Fig. 12. Comparisons of production data before and after history matching.

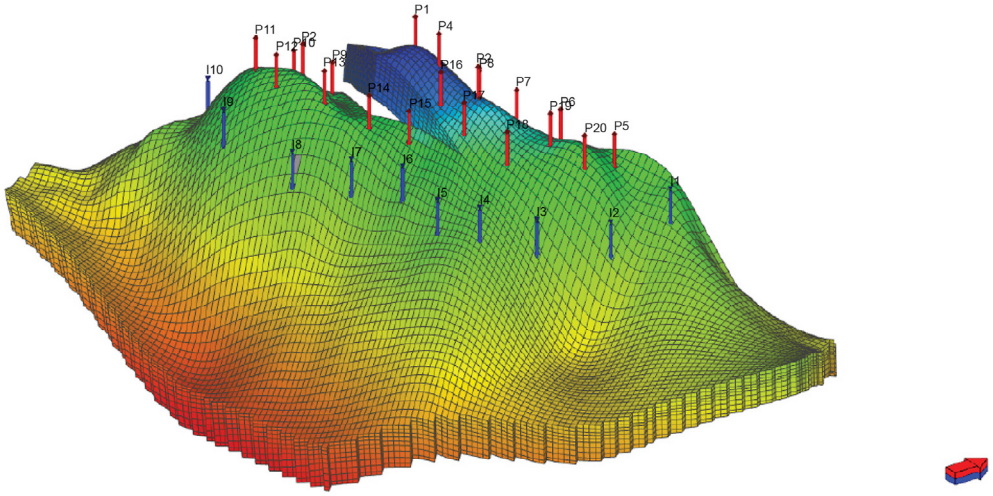

Fig. 13. Top structure of Brugge field.

simulation is not required. The proxy model can give reliable forecasts in a few minutes and reduce uncertainty of reservoir. Besides, the calculation will be more accurate if prior data set are approximately in accordance with the multivariate Gaussian field.

In order to make an intuitive comparison in the following examples, the perturbation on ξ and $\boldsymbol{d}_{\text{obs}}$ vector in Eq. (20) is not taken in consideration. In this way, we can directly predict the posterior state field to perform accuracy of the improved DSI method compared with the true state field. It is noteworthy that we can also calculate the ensemble of posterior forecasts to quantify uncertainty of reservoir on the basis of RML principle.

3. Numerical examples

In this section, two numerical examples are implemented to verify the feasibility of the improved DSI for general reservoir models. The first example is a conventional reservoir with two-phase (oil/water) channel system. The second example is the unconventional fractured reservoir with depletion or water flooding operation.

3.1. Conventional reservoir with high-permeability channels

This section gives an example of waterflooding development for conventional heterogeneous reservoir. The reservoir model has one layer which is divided into 15 × 15 × 1 cells. The size of each cell is 25 m × 2 5 m × 15 m. There is one injector and one producer in the reservoir, which are located on the side of high permeability channel. Fig. 2(a) shows the permeability field of the true model. 100 prior models are generated based on the plane permeability profile, one of them is shown in Fig. 2(b). These prior models all possess the characteristics of high permeability channel, and the true model is not included in the set of prior models.

The initial porosity and oil saturation of those models are 0.2 and 0.8, respectively. The initial reservoir pressure is 25 MPa. The well controls are rate controls for the injector and producer 400 m^3/d, and the production time is set as 450 days. The first 300 days are used for history matching and the last 150 days are used for prediction and verification. The target of history matching are cumulative oil production and cumulative water production.

The reservoir simulator Eclipse is used to calculate the production data and state data (oil saturation and pressure) in the production time for all prior models, which are shown in Fig. 3. In Fig. 3, the prior production data are displayed as grey line and the observed data generated by the true model are indicated by red circles, and the true model data is indicated by the blue curve. In addition, the black line distinguishes the historical period and the forecast-stage period. Obviously, most of the prior production data from prior models cannot match the observed data of the true model.

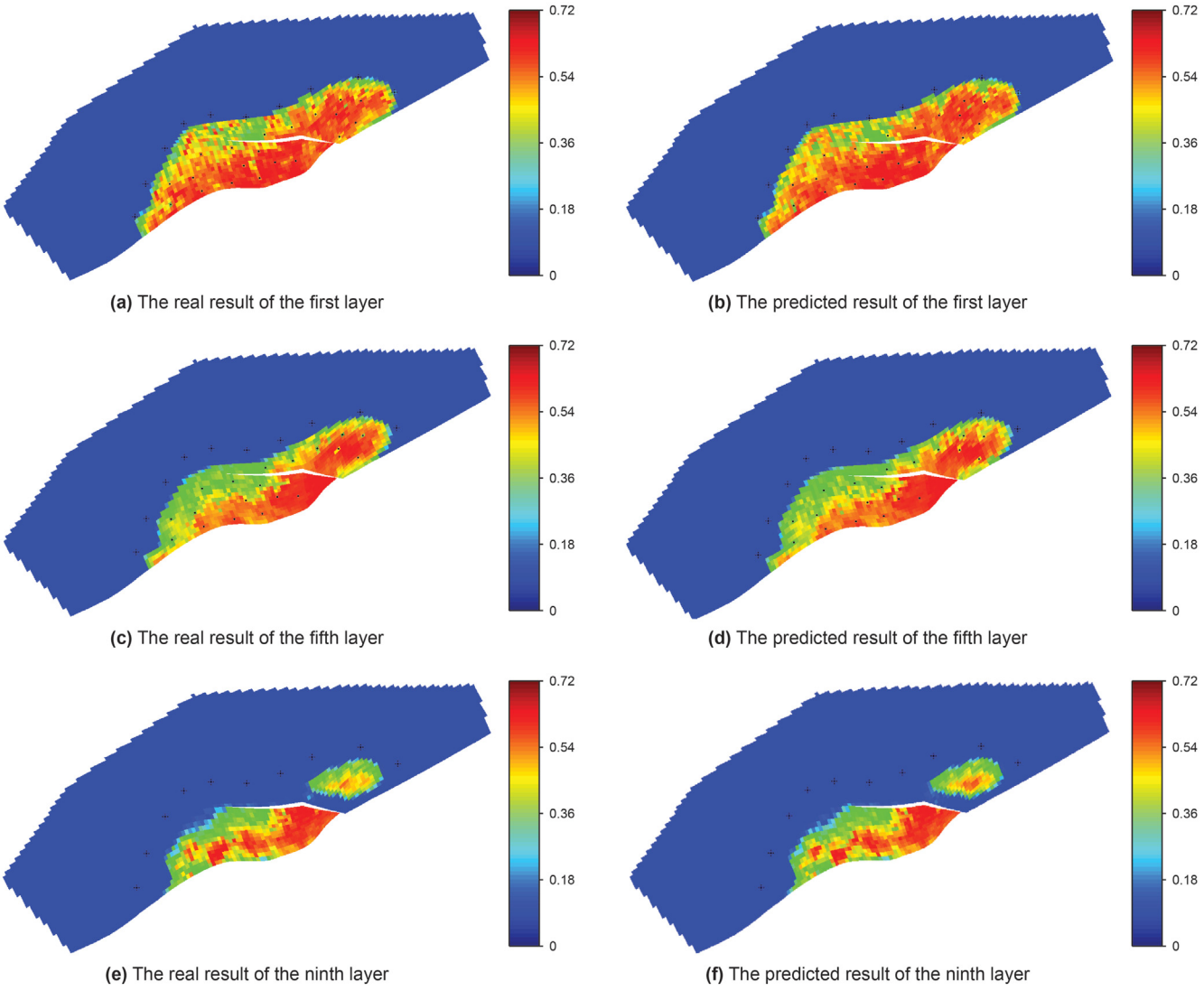

Fig. 14. The comparisons of the oil saturation profiles at the 2700th day.

The history matching results generated by the improved DSI are shown as red curves in Fig. 3. On the one hand, the posterior production data are in good agreement with the observed data and can measure production trends in the future. On the other hand, the posterior state field derived by the conditional proxy model also get good response in general, as shown in Figs. 4 and 5 (The left graph represents the state field simulated by the true model and the right graph represents the state field calculated by the improved DSI). Besides, the improved DSI achieves a better effect of oil saturation prediction compared with pressure prediction. However, the prediction effect of each cell is different. In Figs. 4 and 5, the improved DSI make it better for producer and injector but poor for a few cells. The rough prediction results show that the state field obtained by the improved DSI cannot meet the true field perfectly. But the improved DSI can quickly grasp the basic law of reservoir state field, which is helpful for regulating well controls and new drilling well positions in a certain range.

To study the relationship between the number of prior models and the computational accuracy in this method, we define the relative average error between the predicted and true state fields at N_t time step in Eq. (22). And the relative error vs. the number of prior models is plotted in Fig. 6. In general, the relative error will decrease when the number of prior models increases. Especially, the relative error can be reduced to less than 5% when the number of prior models is only 100. Because the calculation process of this method mainly involves prior model simulations, choosing the appropriate number of prior models is necessary to meet the calculation accuracy requirements and reduce computational cost.

$$E_r = \frac{1}{2 \times N_m}\left(\sum_{i=1}^{2\times N_m}\left(\frac{\boldsymbol{d}_{\text{state,predict},N_t} - \boldsymbol{d}_{\text{state,true},N_t}}{\boldsymbol{d}_{\text{state,true},N_t}}\right)^2\right) \tag{22}$$

3.2. Unconventional reservoir with fractured horizontal well

In this section, examples of depletion and waterflooding operations of unconventional reservoirs with fractured horizontal wells are given to test the performances of presented method. The reservoir model used in this section is divided into $40 \times 25 \times 1$ cells, and the size of each cell is 30 m $\times$ 30 m $\times$ 10 m. Through random sampling of fracture geometry, matrix properties and fracture physical properties, 100 prior models are generated. In the example of depletion development of fractured horizontal

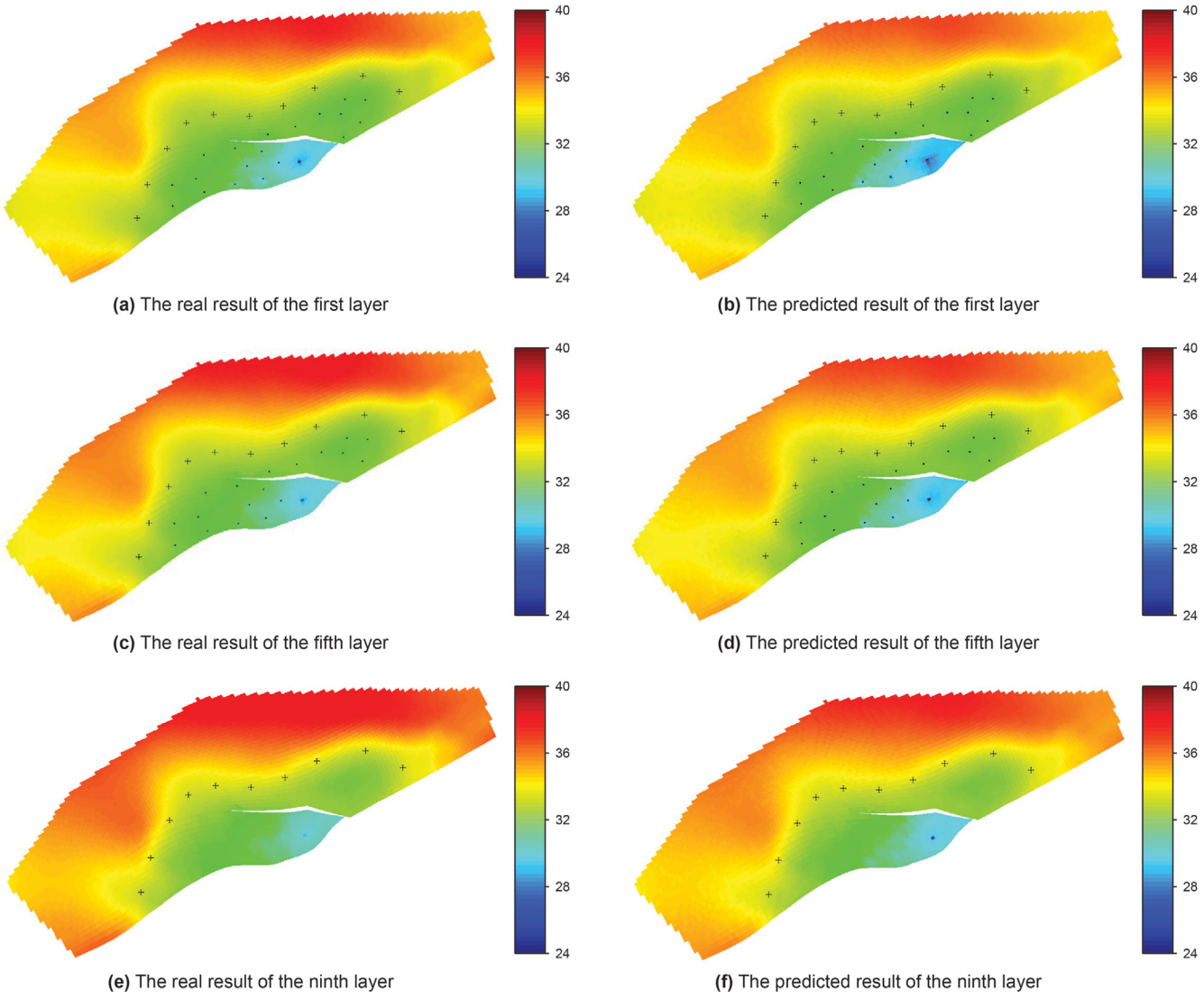

Fig. 15. The comparisons of the pressure profiles at the 2700th day (Pressure, MPa).

wells, the initial reservoir pressure is 20 MPa, the fixed bottomhole pressure of the fractured horizontal well is 12 MPa, and the production time is set as 500 days.

In the example of waterflooding development, there are four water injection wells in the reservoir, which are respectively distributed in the four corners of the rectangular reservoir. The initial reservoir pressure and bottomhole pressure of production wells are the same as those in depletion development. The injection rate of water injection wells is set as 10 m^3/d, and the production time is 2000 days. The first 1200 days are used for history matching and the last 800 days are used for prediction and verification. The embedded discrete fracture model (EDFM) (Rao et al., 2019, 2020a, 2020b; Liu et al., 2020; Zhang et al., 2017, 2019b; Ma et al., 2020) is used for flow simulation (the fracture geometries and matrix-cell permeability profiles in two models are shown in Fig. 7), then the production data (oil/water production rate, cumulative oil/water production, etc.) and pressure and saturation profiles of each prior model are obtained. Fig. 8 shows the production data set obtained from the simulation results of those prior models during waterflooding development.

First of all, the production data is used for history matching to obtain the vector ξ. Then, the vector ξ is used to predict the pressure and saturation profiles of the real model with the reservoir state data of prior models. The predicted results are compared with the reliable real-model EDFM simulation results. The comparison results of the pressure profiles at different time in the case of depletion development are shown in Fig. 9, and the comparisons of the pressure and saturation profiles in the case of waterflooding development are shown in Fig. 10 and Fig. 11. It can be seen that the results predicted by the proposed method are in good agreement with the trustworthy results, which proves that the presented method has a high accuracy.

4. A field case

Brugge field was developed by TNO as a benchmark case for closed-loop reservoir management. Similar to the previously reservoir examples, we generate 100 reservoir realizations based on plane permeability of the true model, the corresponding production data are shown by the grey curve in Fig. 12. This real field is developed by waterflooding with long production history (7200 days divided into 40 control steps) and a large number of wells (20 injectors and 10 producers), as shown in Fig. 13. The reservoir has strong edge and bottom water and injectors are located around the

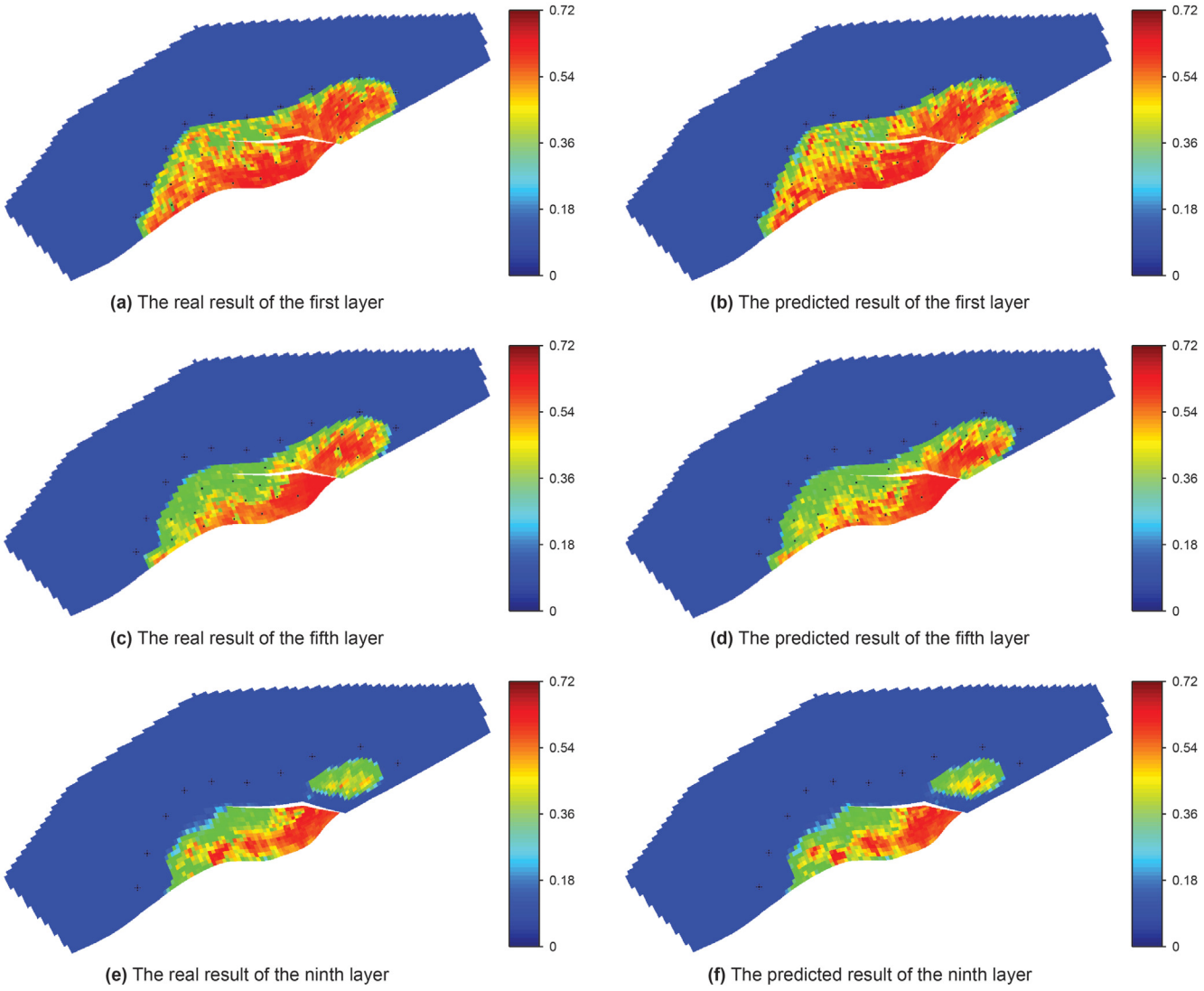

Fig. 16. The comparisons of the oil saturation profiles at the 5400th day.

reservoir for continuous energy supply. And well controls are rate controls for injectors and producers, 5000 m^3/d and 1800 m^3/d, respectively. This reservoir is divided into 139 × 48 × 9 cells. The first 20 steps are used for history matching and the last 20 steps are used for prediction and verification of production data. To reduce the computational cost, we also set the cumulative oil production and water production as the history matching target.

The improved DSI is applied to generate posterior forecasts of state fields via the observed production data. Figs. 14–17 show a comparison of the state fields between the true field and the predicted field at times (2700, 5400) and layers (1, 5, 9). Generally, the predicted state field can match the true state field well. Similar to the previous reservoir examples, the prediction effect of oil saturation is usually better than that of pressure. In practice, accurate saturation forecast can provide more help for engineer to regulate production plans. Moreover, it is importantly to emphasize that there is no repeated simulation in forecast process and the calculation procedure only cost a few minutes.

5. Conclusions

This paper introduces the improved DSI method to predict the state field of reservoir. In this method, served as extra data variables, the reservoir state data is put into the data space but not participated in history matching procedure. Therefore, the improved DSI can not only obtain a posterior production forecast given the observed data, but also predict the pressure and saturation profiles in a few minutes. Throughout the whole paper, several key conclusions are summarized here:

(1) High accuracy: The improved DSI can directly predict the reservoir state fields without inversion of reservoir geological parameters. The numerical examples and field case prove that the predicted pressure and oil saturation are basically consistent with reliable results. Although bad predictions may perform on some cells, but these cells only account for a small part of the whole reservoir model.

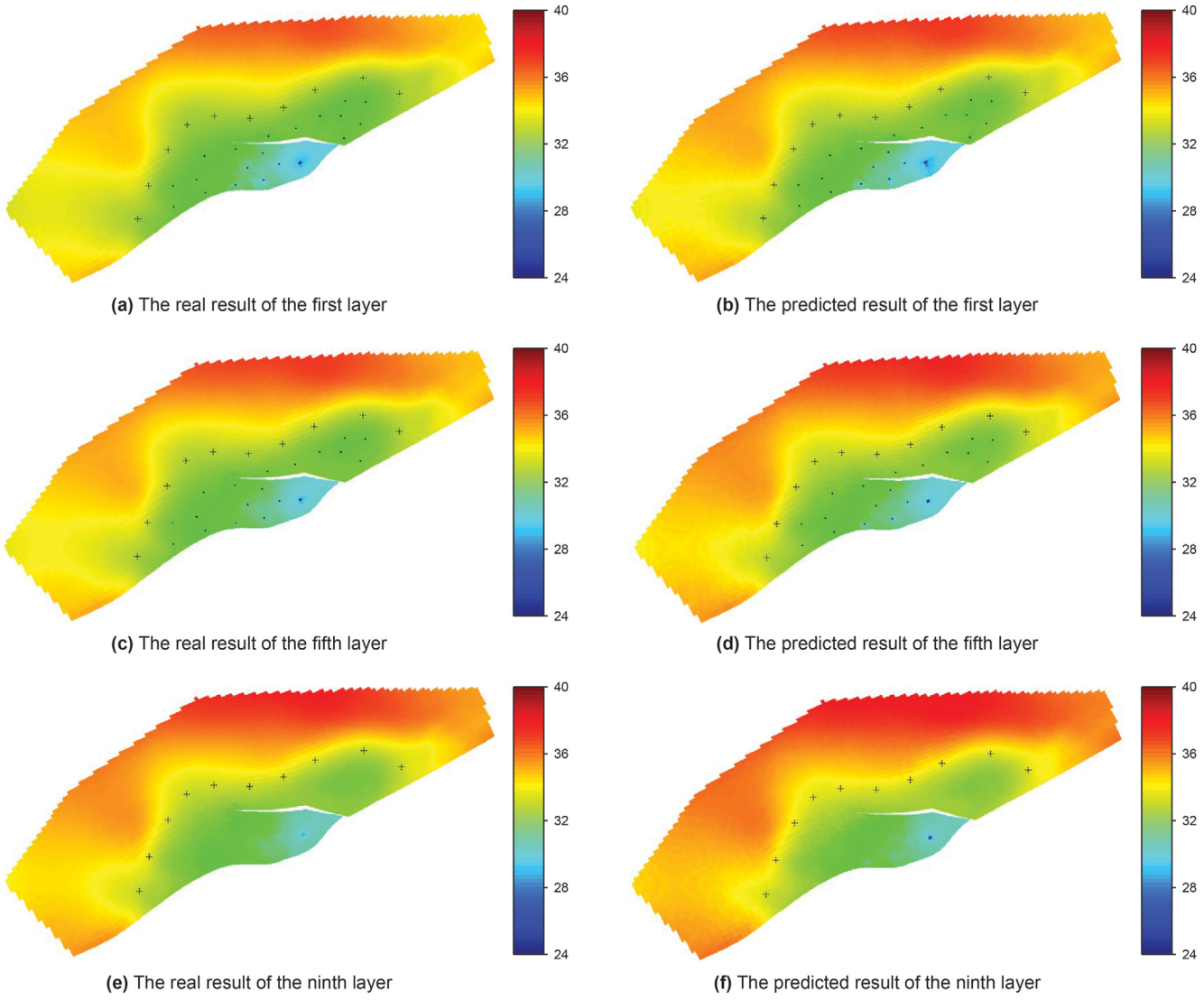

Fig. 17. The comparisons of the pressure profiles at the 5400th day (Pressure, MPa).

(2) High computational efficiency: The improved DSI method can quickly predict production and state fields data without additional simulations when data space is constructed.
(3) SPSA algorithm is adopted for solving this problem to avoid overfitting phenomenon and enhance the practicability of this method. The computational efficiency of SPSA algorithm is lower than gradient-class algorithm, and it can be improved in the future work.

Acknowledgments

This study was supported by Southern Marine Science and Engineering Guangdong Laboratory (Zhanjiang) (No. ZJW-2019-04), and Cooperative Innovation Center of Unconventional Oil and Gas (Ministry of Education & Hubei Province), Yangtze University (No. UOG2020-17), and the National Natural Science Foundation of China (No. 51874044, 51922007). Moreover, the authors wish to thank Luo-Yi Huang, Fei Wang and Jia-Ling Ma for their work in the later revision of this paper.

Appendix. SPSA algorithm

The stochastic gradient of the target function $O(\xi)$ for kth iteration is given by

$$\hat{g}_k\left(\xi^k\right)=\frac{O\left(\xi^k+c_k\Delta_k\right)-O\left(\xi^k-c_k\Delta_k\right)}{2c_k}\Delta_k^{-1} \tag{23}$$

where $\Delta_k \in R^{N_\tau\times 1}$ is the random column vector that satisfies the ± 1 Bernoulli distribution; c_k is a positive coefficient to control the size of perturbation with the fixed value of 0.1. The vector ξ can be updated using steepest descent,

$$\xi^{k+1}=\xi^k+\alpha_{k+1}\hat{\bar{g}}_k\left(\xi^k\right) \tag{24}$$

where α_{k+1} is the iteration step size with the fixed value of 0.5; the average gradient $\hat{\bar{g}}_k(\xi^k)$ is defined by

$$\hat{\bar{g}}_k\left(\xi^k\right)=\frac{1}{n}\sum_{i=1}^{n}\hat{g}_k\left(\xi^k\right) \tag{25}$$

where n is the number of perturbation at each iteration with the fixed value of 5. The iteration step is set to be 50 in this paper. In addition, if the target function value do not decrease for more than

15 iteration steps, the iteration procedure will stop.

References

Albertoni, A., Lake, L.W., 2003. Inferring interwell connectivity only from well-rate fluctuations in waterfloods. SPE Res Eval & Eng 6 (1), 6–16. https://doi.org/10.2118/83381-PA.

Araque-Martinez, A., 1993. Estimation of Autocorrelation and its Use in Sweep Efficiency Calculation. Master's Thesis. University of Texas at Austin, Austin, Texas, USA.

Barros-Griffiths, L., 1998. The Extreme Spearman Rank Correlation Coefficient in the Characterization of the North Buck Draw Field. Master's Thesis. University of Texas at Austin, Austin, Texas, USA.

Brouwer, D.R., Jansen, J.D., van der Starre, S., van Kruijsdijk, C.P.J.W., Berentsen, C.W.J., 2001. Recovery increase through water flooding with smart well technology. In: SPE European Formation Damage Conference, The Hague, Netherlands, May 2001. Society of Petroleum Engineers. https://doi.org/10.2118/68979-MS.

Cao, F., Luo, H., Lake, L.W., 2015. Oil-rate forecast by inferring fractional-flow models from field data with koval method combined with the capacitance/resistance model. SPE Res Eval & Eng 18 (4), 534–553. https://doi.org/10.2118/173315-PA.

Chaki, S., Zagayevskiy, Y., Shi, X., Wong, T., Noor, Z., 2020. Machine learning for proxy modeling of dynamic reservoir systems: deep neural network DNN and recurrent neural network RNN applications. In: International Petroleum Technology Conference, Dhahran, Kingdom of Saudi Arabia, January 2020. Society of Petroleum Engineers. https://doi.org/10.2523/iptc-20118-MS.

Evensen, G., Hove, J., Meisingset, H., Reiso, E., Seim, K.S., Espelid, Ø., 2007. Using the EnKF for assisted history matching of a north sea reservoir model. In: SPE Reservoir Simulation Symposium, Houston, Texas, U.S.A., February 2007. Society of Petroleum Engineers. https://doi.org/10.2118/106184-MS.

Guo, Z., Reynolds, A.C., 2019. INSIM-FT in three-dimensions with gravity. Journal of Computational Physics 380, 143–169. https://doi.org/10.1016/j.jcp.2018.12.016.

Guo, Z., Reynolds, A.C., Zhao, H., 2018. A physics-based data-driven model for history matching, prediction, and characterization of waterflooding performance. SPE J 23, 367–395. https://doi.org/10.2118/182660-PA.

Haugen, V.E., Jensen, N., Lars-Jorgen, E., Geir, B., Aina, M., Flornes, K.M., Geir, N., 2006. History matching using the Ensemble Kalman Filter on a north sea field case. In: SPE Annual Technical Conference and Exhibition, San Antonio, Texas, USA, September 2006. Society of Petroleum Engineers. https://doi.org/10.2118/102430-MS.

Heffer, K.J., Fox, R.J., McGill, C.A., Koutsabeloulis, N.C., 1997. Novel techniques show links between reservoir flow directionality, earth stress, fault structure and geomechanical changes in mature waterfloods. SPE Journal 2 (2), 91–98. https://doi.org/10.2118/30711-PA.

Jansen, F.E., Kelkar, M.G., 1997. Non-stationary estimation of reservoir properties using production data. In: SPE Annual Technical Conference and Exhibition, San Antonio, Texas, October 1997. Society of Petroleum Engineers. https://doi.org/10.2118/38729-MS.

Jiang, S., 2018. Data-space Inversion with Variable Well Controls in the Prediction Period. Master's thesis. Stanford University.

Jiang, S., Sun, W., Durlofsky, L.J., 2019. A data-space inversion procedure for well control optimization and closed-loop reservoir management. Computational Geosciences 24, 361–379. https://doi.org/10.1007/s10596-019-09853-4.

Li, G., Reynolds, A.C., 2011. Uncertainty quantification of reservoir performance predictions using a stochastic optimization algorithm. Computational Geosciences 15 (3), 451–462. https://doi.org/10.1007/s10596-010-9214-2.

Lima, M.M., Emerick, A.A., Ortiz, C.E.P., 2020. Data-space inversion with ensemble smoother. Computational Geosciences. https://doi.org/10.1007/s10596-020-09933-w.

Liu, H., Rao, X., Xiong, H., 2020. Evaluation of CO_2 sequestration capacity in complex-boundary-shape shale gas reservoirs using projection-based Embedded Discrete Fracture Model (pEDFM). Fuel 118201. https://doi.org/10.1016/j.fuel.2020.118201.

Ma, X.P., Zhang, K., Yao, C.J., Zhang, L.M., Wang, J., Yang, Y.F., Jun, Y., 2020. Multiscale-Network structure inversion of fractured media based on a hierarchical-parameterization and data-driven evolutionary-optimization method. SPE Journal 25 (5), 2729–2748. https://doi.org/10.2118/201237-PA.

Naevdal, G., Mannseth, T., Vefring, E.H., 2002. Near-well reservoir monitoring through ensemble Kalman filter. In: SPE/DOE Improved Oil Recovery Symposium, Tulsa, Oklahoma, April 2002. Society of Petroleum Engineers. https://doi.org/10.2118/75235-MS.

Naevdal, G., Johnsen, L.M., Aanonsen, S.I., Vefring, E.H., 2003. Reservoir monitoring and continuous model updating using ensemble Kalman filter. In: SPE Annual Technical Conference and Exhibition, Denver, Colorado, October 2003. Society of Petroleum Engineers. https://doi.org/10.2118/84372-MS.

Nguyen, A.P., Kim, J.S., Lake, L.W., Edgar, T.F., Haynes, B., 2011. Integrated capacitance resistive model for reservoir characterization in primary and secondary recovery. In: SPE Annual Technical Conference and Exhibition, October 30–November 2, 2011. Society of Petroleum Engineers. https://doi.org/10.2118/147344-MS.

Rao, X., Cheng, L., Cao, R., et al., 2019. A modified embedded discrete fracture model to study the water blockage effect on water huff-n-puff process of tight oil reservoirs. Journal of Petroleum Science and Engineering 181, 106232. https://doi.org/10.1016/j.petrol.2019.106232.

Rao, X., Cheng, L., Cao, R., Wu, Y., Liu, H., Zhao, Y., Chen, Y., 2020a. A modified projection-based embedded discrete fracture model (pEDFM) for practical and accurate numerical simulation of fractured reservoir. Journal of Petroleum Science and Engineering 187, 106852. https://doi.org/10.1016/j.petrol.2019.106852.

Rao, X., Zhao, H., Deng, Q., 2020b. Artificial-neural-network (ANN) based proxy model for performances forecast and inverse project design of water huff-n-puff technology. Journal of Petroleum Science and Engineering 195, 107851. https://doi.org/10.1016/j.petrol.2020.107851.

Refunjol, B.T., 1996. Reservoir Characterization of North Buck Draw Field Based on Tracer Response and Production/injection Analysis. Master's thesis. University of Texas at Austin, Austin, Texas, USA.

Sayarpour, M., Kabir, C.S., Lake, L.W., 2009. Field applications of capacitance-resistance models in waterfloods. SPE Reservoir Evaluation & Engineering 12 (6), 853–864. https://doi.org/10.2118/114983-PA.

Spall, J.C., 2000. Adaptive stochastic approximation by the simultaneous perturbation method. IEEE Transactions on Automatic Control 45 (10), 1839–1853. https://doi.org/10.1109/TAC.2000.880982.

Spall, J.C., 1992. Multivariate stochastic approximation using a simultaneous perturbation gradient approximation. IEEE Transactions on Automatic Control 37 (3), 332–341. https://doi.org/10.1109/9.119632.

Sun, W., Durlofsky, L.J., 2017. A new data-space inversion procedure for efficient uncertainty quantification in subsurface flow problems. Mathematical Geosciences 49 (6), 679–715. https://doi.org/10.1007/s11004-016-9672-8.

Sun, W., Hui, M., Durlofsky, L.J., 2017. Production forecasting and uncertainty quantification for naturally fractured reservoirs using a new data-space inversion procedure. Computational Geosciences 21 (5), 1443–1458. https://doi.org/10.1007/s10596-017-9633-4, 2017b.

Sun, W., Durlofsky, L.J., 2019. Data-space approaches for uncertainty quantification of CO_2 plume location in geological carbon storage. Advances in Water Resources 234–255. https://doi.org/10.1016/j.advwatres.2018.10.028.

Tiab, D., Dinh, A.V., 2008. Inferring interwell connectivity from well bottomhole-pressure fluctuations in waterfloods. SPE Res Eval & Eng. 11 (5), 874–881. https://doi.org/10.2118/106881-PA.

Wang, C., Li, G., Reynolds, A.C., 2009. Production optimization in closed-loop reservoir management. SPE J 14 (3), 506–523. https://doi.org/10.2118/109805-PA.

Yousef, A.A., Gentil, P.H., Jensen, J.L., Lake, L.W., 2005. A capacitance model to infer interwell connectivity from production and injection rate fluctuations. In: SPE Annual Technical Conference and Exhibition, Dallas, Texas, October 2005. Society of Petroleum Engineers. https://doi.org/10.2118/95322-MS.

Zhang, L.M., Cui, C.Y., Ma, X.P., Sun, Z.X., Zhang, K., 2019b. A fractal discrete fracture network model for history matching of naturally fractured reservoirs. Fractals 27 (1), 1940008. https://doi.org/10.1142/S0218348X19400085.

Zhang, Q., Wei, C., Wang, Y., Du, S., Zhou, Y., Song, S., 2019a. Potential for prediction of water saturation distribution in reservoirs utilizing machine learning methods. Energies 12 (19). https://doi.org/10.3390/en12193597.

Zhang, K., Zhang, X.M., Zhang, L.M., et al., 2017. Assisted history matching for the inversion of fractures based on discrete fracture-matrix model with different combinations of inversion parameters. Computational Geosciences 21, 1365–1383. https://doi.org/10.1007/s10596-017-9690-8.

Zhao, H., Kang, Z., Zhang, X., Sun, H., Cao, L., Reynolds, A.C., 2016. A physics-based data-driven numerical model for reservoir history matching and prediction with a field application. SPE J 21 (6), 2175–2194. https://doi.org/10.2118/173213-PA.

Zhao, H., Xu, L., Guo, Z., Zhang, Q., Liu, W., Kang, X., 2020. Flow-path tracking strategy in a data-driven interwell numerical simulation model for waterflooding history matching and performance prediction with infill wells. SPE J 25 (2), 1007–1025. https://doi.org/10.2118/199361-PA.